Title: "An adaptive pneumatic suspension based on the estimation of the excitation frequency"

Authors: Nieto A.J., Morales A.L., Trapero J.A., Chicharro, J.M., Pintado P.

JOURNAL OF SOUND AND VIBRATION, 307, pp. 365-378 (2011)

Keywords:

Pneumatic suspension, stiffness, transmissibility

DOI: 10.1016/j.jsv.2010.11.009

An adaptive pneumatic suspension based on the estimation of the excitation frequency

A.J. Nieto[a], A.L. Morales[a], J.R. Trapero[b], J.M. Chicharro[a], P. Pintado[a]

[a] *Área de Ingeniería Mecánica, E.T.S.I. Industriales (Universidad de Castilla - La Mancha), Avda. Camilo José Cela s/n, 13071, Ciudad Real (Spain)*
[b] *Department of Management Science, Lancaster University, Lancaster, LA1 4YX, United Kingdom*

Abstract

A pneumatic suspension that can adapt itself to the incoming vibration is presented in this paper. A switching control strategy between two different configurations is proposed and studied. The objective is to avoid undesirable resonant frequencies. The control procedure is based on the pre-knowledge of the incoming vibration frequency, and when this frequency is unknown, a very efficient prediction technique is used. The results show that the adaptable suspension has improved performance as compared to any of its passive counterparts. The transient response when switching typically takes less than three cycles and does not hinder the suspension performance.

Keywords: Pneumatic suspension, control strategy, transients, signal estimation.

Email address: AntonioJavier.Nieto@uclm.es (A.J. Nieto)

PACS codes: 47.15.K-, 91.55.Ax, 47.27.nf

NOMENCLATURE

A_s	Spring effective area [m^2]
C_r	Restriction coefficient [$N^5/m/s$]
D_p	Pipe's cross section diameter [m]
f_n	Resonant frequency of the pneumatic suspension [Hz]
f	Force exerted at the air spring [N]
g	Acceleration due to gravity [m/s^2]
K	Pneumatic suspension total linear stiffness [N/m]
K_{AS}	Linear stiffness of the air spring due to effective area variations.
K_S	Air spring linear stiffness [N/m]
K_{VS}	Linear stiffness of the air spring due to volume variations [N/m]
K_{VSR}	Linear stiffness of the suspension due to volume variations [N/m]
l_p	Pipe length [m]
M	Sprung mass [kg]
p_r	Gage pressure at the reservoir [bar]
p_s	Gage pressure at the air spring [bar]
V_r	Reservoir volume [m^3]

V_s	Air spring volume [m^3]
V_{sr}	Reservoir plus spring volume [m^3]
x	Absolute response [m]
y	Excitation [m]
z	Suspension height [m]
z_0	Initial height for the air spring [m]
γ	Specific heat ratio
μ	Dynamic viscosity of air [Pa·s]
ξ	Adimensional damping coefficient
ω_{tr}	Transition frequency [rad/s]

1. Introduction

Pneumatic systems are used for vibration isolation in many applications. One of the most prominent advantages over metallic counterparts is the fact that the main natural frequency of the system can be made independent of sprung mass. Despite the widespread use of pneumatic vibration isolation systems, the possibilities of using the pneumatic configuration as an adaptive, semi-active or even active system have not been sufficiently studied.

Many works incorporate pneumatic suspensions as a solution for vibration

isolation of mobile machine seats. Hostens presented an improved design of air suspension for agricultural machines seats [1]. The authors used an air spring, an additional reservoir to lower the system natural frequency and a throttle valve in order to obtain air damping. The results show reduction of harmful vibrations transmitted to the driver but with no contribution to minimize the suspension deflection. A modified passive air suspension in presented in [2] taking as a basis a simple passive air suspension. This work focuses on the simultaneous effect of an additional air reservoir placed in the air-spring by the throttle and a change in the characteristics of a shock-absorber. The results of this work contribute to better health protection of the operator while maintaining the controllability of the working machine.

Other works tackling this same problem try to model and control the vibro-isolating properties of an active seat suspension in response to varying load mass [3]. The results show quite success with a reduction of the amplitude at resonance by about 50 percent in comparison to passive systems. Following the seat suspensions problem, other authors focus their work in the infra-narrow band of 0.5-5 Hz which is especially vibrosensitive [4]. This work presents an approach for the position control of a vibration isolating mechanism with the concept of negative stiffness where the standard controlled

devices are ineffective. The approach is based on the stiffness minimization by coupling a mechanism with an air spring with adjustable "negative" stiffness. The results ensure immobility under vibrations beginning with infra-frequencies close to zero Hz and stabilization and shock-free motion under impulsive excitation.

The analysis of semi-active suspensions has focused mainly on modifying the damping characteristics of the system, either by mechanical actuation on the damper, or by using magnetorheological (MR) or electrorheological (ER) fluids. It is not difficult to find examples in the literature [5, 6, 7] showing the merits of hybrid suspensions combining passive elements along with electromagnetic devices as active elements. Purely active systems have also been considered but they all suffer from the seemingly unavoidable drawback of energy consumption, although there have been some attempts to look for ways to self-power the main control actuator [8].

Many semi-active control strategies have been studied in the last three decades: the very well-known "skyhook" approach has been used in many occasions [9, 10]; hybrid strategies, that combine adaptive controllers with filtered-x least mean squares (FXLMS) algorithms [11], have also been considered; and sliding mode control [12, 13] has been applied to several fields

including vibration isolation.

Modifying stiffness has been traditionally more difficult than modifying damping. Nevertheless, this paper will show that this is not the case when using pneumatic systems, and that the possibility of modifying stiffness and, thus, natural frequency, suggests a straightforward control strategy. The approach is based on switching between two different configurations in order to avoid undesirable resonant frequencies. The control procedure requires the pre-knowledge of the input frequency which is estimated using very efficient algebraic predictors. The methods were originally developed by Fliess and Sira-Ramírez in [14] to tackle the problem of parameter estimation in linear continuous-time systems. A theoretical background with several examples is available in [15]. This novel approach has also been successfully applied to monitor the vibration frequency of a single-link flexible manipulator in [16]. Additionally, closed-loop [17] and feedforward [18] adaptive controllers were developed employing this algebraic identification in order to suppress undesirable vibrations which appear in very light weight structures. The technique obtains fast estimations [19], does not rely on the knowledge of the statistical properties of the noise, and keeps the "true" physical nature of the unknown parameters that can even be altered while sampling [20].

The objectives of this papers are mainly three: i) the development of an inexpensive and easily controlled adaptive pneumatic system capable of modifying stiffness and, thus, natural frequency, ii) the implementation and verification of a suspension control strategy based on quick switching between two different configurations, and iii) feeding the control procedure with very efficient algebraic predictors to determine the input frequency.

The outline of the paper is as follows. The suspension model and the control strategy are presented in Section 2. Section 3 shows an indirect measurement method to quantify parameters that affect the control strategy, whereas Section 4 outlines a fast time-domain technique for input signal identification. The results of simulations and tests using the proposed adaptive pneumatic suspension are described in Section 5 highlighting its improved performance. Switching between suspension configurations may translate into undesirable time delays in the response, but this question is tackled in Section 6 to show that the delays do not hinder performance. Finally, the main conclusions are summarized in Section 7.

2. Theoretical background

2.1. Pneumatic suspension model

The pneumatic suspension behavior is modeled by taking into account the dynamics of the sprung mass as well as the fluid dynamics of the air inside the pneumatic system. This system, in the configuration under study, is composed of an air spring, a rigid reservoir and a pipe connecting the two as can be seen in Fig. 1. The authors have developed and published [21] a validated model for a pneumatic suspension of this type. A brief description of the model follows.

Three assumptions have been made for the closed system that includes the air spring and reservoir. The first of them is the assumption of isothermal compression and expansion of the air. The suspension air temperature was monitored experimentally in working conditions by means of a thermocouple. The results therefore supported the hypothesis of an isothermal transformation. The second is the assumption that the air behaves as an ideal gas. The last assumption is the consideration of an incompressible-fully-developed-laminar flow (Hagen-Poiseuille flow), in particular, Mach number $M < 0.3$ and Reynolds number $Re < 2300$, which is reasonable taking into account the size of the pipes and the amplitude and frequency of the excitation signal [22].

Support for these assumptions may be found in [21]. Under these simplifications, the system dynamics is described by the following set of differential equations:

$$\begin{cases} \dot{p}_s = -\dot{p}_r \frac{V_r}{V_s} - V_s' \frac{p_s}{V_s}(\dot{x} - \dot{y}) \\ \dot{p}_r = -\frac{\gamma C_r}{2V_r}\left({p_r}^2 - {p_s}^2\right) \\ M\ddot{x} = \dot{p}_s A_s + p_s A_s'(\dot{x} - \dot{y}) = \dot{f} \end{cases} \tag{1}$$

where the unknown functions of time are the pressure in the air spring (p_s), the pressure in the reservoir (p_r) and the absolute sprung mass displacement (x). The rest are either known parameters like the sprung mass (M), the reservoir volume (V_r), the restriction coefficient (C_r), which can be determined from other parameters as will be shown in this section; or a known function of time like the excitation displacement (y); or functions that can be experimentally determined, like the air spring effective area ($A_s(z)$) and volume ($V_s(z)$). These latter functions depend on the air spring height z, which is defined as the difference between $x(t)$ and $y(t)$ plus an initial air spring height z_0. Finally, the apostrophe on $A_s(z)$ and $V_s(z)$ denotes the derivative of these functions with respect to the air spring height.

The size of the pipe and the air viscosity determine the restriction coef-

ficient (C_r) [23]:

$$C_r = \frac{\pi D_p^4}{128 \mu l_p} \tag{2}$$

where l_p is the pipe length, D_p its diameter, and μ is the dynamic viscosity of air.

The system of differential equations just described is the result of rearranging the continuity equation of the mass flow in the pipe, the discharge equation from the pipe to the reservoir (or air spring), and Newton's second law applied to the sprung mass. Details of this derivation may be found in [21].

A linear version of the system of differential equations is obtained by carrying out a first-order Taylor series expansion, and this linear system may be transformed into the following set of algebraic equations by using the Laplace transform:

$$\begin{cases} sP_s(s) + \frac{V_r}{V_s^{st}} sP_r(s) + \kappa \frac{P_s^{st}}{V_s^{st}} s(X(s) - Y(s)) = 0 \\ sP_r(s) + \frac{\gamma C_r P_s^{st}}{V_r} (P_r(s) - P_s(s)) = 0 \\ Ms^3 X(s) - A_s^{st} sP_s(s) - \lambda P_s^{st} s(X(s) - Y(s)) = 0 \end{cases} \tag{3}$$

where upper case functions represent the Laplace transform of its lower case counterpart, and s is the Laplace domain variable. The superscript st denotes the static equilibrium point (around which the linear version of the model is

built), and the parameters λ and κ are, respectively, $\lambda = A_s^{'st}$ and $\kappa = V_s^{'st}$. Rearranging some of the above terms, it is possible to obtain the transfer function between the exerted force and the air spring height, that is, the stiffness transfer function of the pneumatic suspension:

$$\frac{F(s)}{Z(s)} = -\frac{s\left(K_{AS} + K_{VS}\right) + WK_{VS}\left(1 + \frac{K_{AS}}{K_{VSR}}\right)}{s + W\left(\frac{K_{VS}}{K_{VSR}}\right)} \tag{4}$$

where, as indicated above, $F(s)$ and $Z(s)$ are the Laplace transforms of $f(t)$ and $z(t)$, respectively, and W is defined as $W = \gamma C_r P_s^{st}/V_r$. The linear stiffness terms K_{AS}, K_{VS}, and K_{VSR} are:

$$K_{AS} = -P_s^{st}\lambda \tag{5}$$

$$K_{VS} = \frac{P_s^{st}A_s^{st}}{V_s^{st}}\kappa \tag{6}$$

$$K_{VSR} = \frac{P_s^{st}A_s^{st}}{V_s^{st} + V_r}\kappa \tag{7}$$

The transfer function between the response and the excitation signal is given by:

$$\frac{X(s)}{Y(s)} = \frac{s\left(\frac{K_{AS}+K_{VS}}{M}\right) + W\frac{K_{VS}}{M}\left(1 + \frac{K_{AS}}{K_{VSR}}\right)}{s^3 + s^2\left(W\frac{K_{VS}}{K_{VSR}}\right) + s\left(\frac{K_{AS}+K_{VS}}{M}\right) + W\frac{K_{VS}}{M}\left(1 + \frac{K_{AS}}{K_{VSR}}\right)} \tag{8}$$

again, $X(s)$ and $Y(s)$ are the Laplace transforms of $x(t)$ and $y(t)$, respectively. These results are used next to design a control strategy in order to enhance the performance in vibration isolation.

2.2. Control strategy

Fig. 2 plots the transfer function of Eq.(8) using the parameters specified in Table 1 for two different values of the restriction coefficient: $C_r \approx 10^{-5}$ m^5/Ns and $C_r \approx 10^{-8}$ m^5/Ns. The plot suggests a control strategy for cases in which the excitation frequency is known or can be estimated. The strategy consists in using one connecting pipe, the one with the smallest C_r for frequencies bellow ω_{tr} (the frequency where both transmissibility functions intersect, Fig. 2), and the other connecting pipe, the one with the highest C_r for frequencies above ω_{tr}. Switching from one pipe to the other can be easily done by opening and closing control valves in each line. The authors have used this strategy for the case of unbalanced rotating machinery subjected to frequent start-stop cycles [24], and the objective now is to adapt the concept and the design to more general situations.

The point where both transmissibility functions intersect (labeled A in Fig. 2) is independent of the restriction coefficient, which means that any other connecting pipe that one may try to use will yield a transmissibility function intersecting all others at point A. The frequency for which the transmissibility modulus is independent of the restriction coefficient can be easily

derived as:

$$\omega_{tr} = \sqrt{\frac{K_S}{M}\frac{2K}{K_S + K}} \tag{9}$$

where $K_S = K_A + K_{VS}$ and $K = K_A + K_{VSR}$, while the value of the transmissibility modulus at this transition frequency is:

$$\left|\frac{X}{Y}\right|_{tr} = \frac{K_S + K}{K_S - K} \tag{10}$$

This modulus is a function of stiffness K_S and stiffness K. The greater the value of K_S and the smaller the value of K, the smaller the modulus. Therefore, the selection of the suspension elements must be aimed at separating these two stiffness parameters as much as possible. In other words, one must seek the greatest possible distance between the eigenfrequency values corresponding to the smallest and highest C_r coefficients in the transmissibility diagram by maximizing and minimizing the values of K_{VS} and K_{VSR}, respectively. This involves reducing the air spring volume V_s and increasing the reservoir volume V_r. Fig. 3 shows the suspension behavior when these changes are considered. This plot helped us select the parameter values specified in Table 1.

3. Influence of mass on the control strategy

The way in which the control strategy needs to be modified in order to account for changes in sprung mass is analyzed in this section.

The suspension transmissibility modulus diagram is determined for the following sprung masses: 70 kg, 100 kg, 115 kg and 130 kg. The results of this simulation can be seen in Fig. 4(a) for both suspension configurations. The plot shows no dependance of the transmissibility modulus at each ω_{tr} on the sprung mass value. This is a fortunate fact because it implies that the controlled vibration is not going to change dramatically with changes in sprung mass. Nevertheless, changes in the sprung mass involve changes in ω_{tr}. These statements can also be inferred from Eqs. (9) and (10). Therefore, knowledge of the sprung mass is needed if one wants to implement the argued control strategy, but it will be shown next that the sprung mass can be determined by adjusting the air spring height and pressure in static conditions.

The following test has been devised to this end. The suspension is filled up to an initial pressure. The air spring height is varied slowly up and down $z_0 \pm 25$ mm. Height and pressure are measured with a linear variable displacement transducer (LVDT) and a pressure gage, respectively. The

procedure is repeated for several values of initial pressure, and the results are arranged as a regression of the force as a function of P_{s0} and z in Fig. 4(b). Since this force equals the sprung mass times the acceleration of gravity in static conditions, Fig. 4(b) is also a plot of mass as a function of P_{s0} and z. Consequently, a pressure gage (Sensotec Sensors 0-6 bar) to measure the suspension air pressure in static conditions and an LVDT (Schaevitz Sensors core rod $\pm$50 mm) to determine the air spring height, suffice to determine the sprung mass from the map in Fig. 4, and this value can be readily used to determine ω_{tr} from Eq. (9).

4. Input signal identification

As argued before, the proposed control strategy basically compares the input signal frequency with ω_{tr} and chooses the appropriate suspension configuration between the two possibilities. The task is straightforward in cases, like those considered in [24], in which the input signal frequency can be easily known. Otherwise, and in order to retain the basic control concept, one needs to implement a procedure to estimate the input frequency.

One approach to estimate the input frequency would be to conduct a frequency analysis, but these methods are soon discarded since they cannot

be performed fast enough to agilely change the suspension configuration. A more suitable approach is to use time domain signal estimation techniques like those considered in [20], [19] and [16]. Details of the techniques may be found in the aforementioned references, but a brief outline of the procedures will be presented next for the cases of sinusoidal and chirp signals.

Let us first consider the case in which the input signal can be represented by a sinusoidal function of unknown amplitude, frequency and phase blurred by a highly fluctuating random process of unknown statistics. This input signal may be expressed as:

$$y(t) = A\sin(2\pi f t + \phi) + e(t) \tag{11}$$

where A, f and ϕ are, respectively, the (constant and positive) unknown amplitude, frequency and phase. For the sake of simplicity, parameter ϕ is assumed strictly positive and less than 2π. The additive signal $e(t)$ represents the fluctuating process, the mean of which is assumed to be zero.

The algebraic frequency estimator proposed in [16] is given by:

$$f^2 = \frac{1}{(2\pi)^2}\frac{(g \cdot n)(t)}{(g \cdot d)(t)} \tag{12}$$

where g is a low-pass filter (Heaviside type function) to reduce the high frequency noise (the Laplace transform of which is $\mathcal{L}\{g(t)\} = G(s) = \frac{1}{s^2}$),

and variables $n(t)$ and $d(t)$ are obtained from the input signal $y(t)$ after solving the following system of differential equations:

$$\begin{aligned} n(t) &= -[x_1 + t^2 y(t)] & d(t) &= x_3 \\ \dot{x}_1 &= x_2 + 4ty(t) & \dot{x}_3 &= x_4 \\ \dot{x}_2 &= 2y(t) & \dot{x}_4 &= t^2 y(t) \end{aligned} \tag{13}$$

As an example, Fig. 5(a) depicts one cycle of a harmonic signal in which $A = 1$ mm, $f = 2$ Hz and $\phi = 0$ rad, with a superposed normally distributed noise $e(t)$ with zero mean and 0.005 mm^2 variance. Fig. 5(b) shows the frequency estimated using the procedure just outlined (in solid line) and the correct value in dashed line. The figure shows that the estimation reaches the correct value in approximately 0.3 seconds, and it is worth emphasizing that this time is less than the harmonic signal period.

Let us now consider the case in which the input signal can be represented by a chirp signal of unknown amplitude and frequency evolution, again blurred by a highly fluctuating random process of unknown statistics. This input signal may be expressed as:

$$y(t) = A\sin(\varphi(t)) + e(t) \tag{14}$$

where $\varphi(t)$ is a quadratic function of time $\varphi(t) = \varphi_0 + \varphi_1 t + \varphi_2 t^2$, with φ_0,

φ_1, and φ_3 unknown constants; A is a positive unknown constant amplitude and $e(t)$ is a noise of zero mean.

The instantaneous frequency is given by:

$$\frac{d\varphi(t)}{dt} = \varphi_1 + 2\varphi_2 t \tag{15}$$

Thus, the objective is just the estimation of the unknown parameters φ_1 and φ_2. To that end, it is convenient to observe that the noise-free chirp signal in Eq.(14) satisfies the following differential equation:

$$\dddot{y} + \dot{\varphi}(t)^2 \dot{y}(t) + 3\dot{\varphi}(t)\ddot{\varphi}(t)y(t) = 0 \tag{16}$$

which, after applying the Laplace transform, yields:

$$\begin{aligned}(2\varphi_1\varphi_2 + \varphi_1^2 s + s^3)Y(s) - 4\varphi_2(\varphi_2 + \varphi_1 s)\frac{dY(s)}{ds} + 4\varphi_2^2 s\frac{d^2Y(s)}{ds^2} \quad &= \\ \ddot{y}(0) + y(0)\varphi_1^2 + \dot{y}(0)s + y(0)s^2 \qquad &(17)\end{aligned}$$

Introducing the following new variables:

$$\begin{aligned}\theta_1 &= \ddot{y}(0) + \varphi_1^2 y(0) = 2\varphi_2 A\cos\varphi_0 & \theta_4 &= -\varphi_1^2 \\ \theta_2 &= \dot{y}(0) = \varphi_1 A\cos\varphi_0 & \theta_5 &= 2\varphi_1\varphi_2 \\ \theta_3 &= y(0) = A\sin\varphi_0 & \theta_6 &= -4\varphi_2^2 \end{aligned} \tag{18}$$

one may write a system of (six) equations which is linear in the unknown

variables θ_i, $i = 1, 2, \ldots, 6$ (see [20], [25] and [15] for details):

$$s^{-\nu}\frac{d^k}{ds^k}\left\{\theta_1 + \theta_2 s + \theta_3 s^2 + \theta_4 s Y(s) + \theta_5(2s\frac{dY(s)}{ds} - Y(s))\right\}$$
$$+s^{-\nu}\frac{d^k}{ds^k}\left\{\theta_6(s\frac{d^2Y(s)}{ds^2} - \frac{dY(s)}{ds})\right\} = s^{-\nu}\frac{d^k}{ds^k}s^3Y(s), \qquad k = 0, 1, \ldots, 5 \tag{19}$$

In order to avoid positive exponents of the complex variable s associated with time derivatives (note that time derivatives are noise amplifiers), the linear system is multiplied by $s^{-\nu}$. Additionally, in algebraic estimation literature is common to apply a low pass filter to both terms in Eq.(19). This invariant filtering enhances the estimation. An analysis of the impact of this kind of filtering is done in [26]. Considering the aforementioned reasons the value of ν can be set equal to 5. Applying a low pass filter and taking the inverse Laplace transform of the system, one may solve for the six unknowns θ_i, $i = 1, 2, \ldots, 6$, from which φ_1 and φ_2 are readily obtained.

As an example, Fig. 6(a) depicts a chirp signal with $A = 1$ mm, $\varphi_0 = 1$ rad, $\varphi_1 = 0.5$ rad/s, and $\varphi_2 = 0.25$ rad/s^2, polluted by a normally distributed noise $e(t)$ with zero mean and 0.005 mm^2 variance. Fig. 6(b) shows the estimated φ_1 in solid line, as well as the correct value in dashed lines. Likewise, Fig. 6(c) shows the estimated (solid line) and correct (dashed line) φ_2. The instantaneous frequency is determined from φ_1 and φ_2 (Eq. (15))

and its estimation shown in Fig. 6 (d). It can be seen in these figures that the estimation process converges almost exactly to the desired values in less than 3 seconds.

5. Application to vibration control

In order to use the identification processes of the previous section for vibration control, some a priori information on the type of excitation is needed. For the cases considered in this paper, and before attempting to identify the input frequency, one would need to decide whether the excitation can be roughly represented by a piecewise harmonic signal of nearly constant frequency (within each piece) or if it can be represented by a chirp signal of rising frequency. No other type of input has been considered in this work although similar identification procedures could be devised for these cases. But regardless of the number of possible types of input, the specific type to be identified and controlled needs to be known ahead of time. The strategy presented here cannot, therefore, be used in the most general case, although it is also true that there are some practical situations in which knowledge of the type of input is feasible. In any case, the study presented here should be taken as a first step towards more general situations. The details of the

process are beyond the scope of this work, but it can be said that it will involve estimation of the excitation power spectral density (PSD), as well as criteria to switch between pipes of different sizes. To this end, real-time PSD estimation techniques (as proposed in [27]) will be needed.

Fig. 7 shows the block diagram of the explained algebraic estimator that will be applied to the pneumatic suspension system. Consider first the case in which the excitation is a piecewise harmonic signal like that depicted in Fig. 8(a). The first and third segments of the signal are similar, their amplitude and frequency being 3 mm and 2 Hz, respectively. The segment in between has an amplitude of 1.5 mm and a frequency of 4.5 Hz. A uniform normal noise of zero mean and 0.005 mm^2 variance is added throughout. Fig. 8(b) shows the estimated frequency as a function of time. The figure shows that the predictor responds quickly to changes in input frequency, the delay being nearly negligible.

This chain of harmonic signals was fed as input to the suspension model given by Eq. (1). Three configurations were used in the simulations: two passive configurations in which C_r is kept constant throughout the simulation ($C_r \approx 10^{-8}$ m^5/Ns in one case, and $C_r \approx 10^{-5}$ m^5/Ns in the other), and an active configuration in which C_r is modified according to the control strategy

outlined in Section 2.2 using the predicted input frequency. The results are plotted in Fig. 8(c). It is clear from this figure that having the possibility of modifying the suspension configuration greatly reduces the sprung mass response.

The same test was conducted in the laboratory by feeding the input signal to a hydraulic unit connected to the bottom side of the air spring. The sprung mass (115 kg) had been determined previously as outlined in Section 3: by measuring the air pressure in the bellows that allowed lifting the sprung mass up to the selected height z_0. These two magnitudes are, respectively, 2 bar and 105 mm. After this step, the hydraulic unit starts reproducing the input signal. The sprung mass displacement signal is captured by means of an LVDT. This signal is analyzed using the identification techniques described in section 4, and the predicted frequency is compared with the value of ω_{tr} obtained from the measured sprung mass. When this comparison generates a switch order, a digital signal is sent to the solenoid valves (function 2/2 way) that open and close the connecting pipes. Fig. 8(d) shows the experimental results which, as can be seen, are in very good agreement with those obtained in the simulations.

Consider now the case in which the excitation is a chirp signal like that

depicted in Fig. 9(a): a constant amplitude signal (A =1.5 mm) the frequency of which rises linearly from 0.5 to 10 Hz in 200 s. The frequency estimation is plotted in Fig. 9(b) as a function of time. Since it takes less than three seconds to converge to the correct frequency, the suspension behaviour is hardly influenced by the configuration selected in such a short period of time. Again, three configurations were used in simulations and tests: two passive configurations of constant C_r ($C_r \approx 10^{-8}$ m^5/Ns in one case, and $C_r \approx 10^{-5}$ m^5/Ns in the other), and an active configuration in which C_r is modified using the predicted input frequency. The results are plotted in Fig. 9(c) (for the passive cases) and Figs. 9(d) and 9(e) (for the numerical and experimental controlled response). It is clear from this figure that having the possibility of modifying the suspension configuration greatly reduces the sprung mass response.

6. Study of transients

The control strategy involves switching between two different configurations at specific times. The switching will generate transient responses that are worth considering. The transition is modeled analytically by specifying the sprung mass position and velocity when the switching occurs as initial

conditions for the new configuration: x_0, $\dot{x}_0$. These initial conditions are taken into account when obtaining the Laplace transform of response $x(t)$, and this transform is used to derive the transient version of the transmissibility transfer function for the new suspension configuration which can be written as:

$$\left.\frac{X(s)}{Y(s)}\right|_t = \frac{s^2 x_0 + s\left(\dot{x}_0 + W\frac{K_{VM}}{K_{VMD}}x_0\right) + W\frac{K_{VM}}{K_{VMD}}\dot{x}_0}{s^3 + s^2\left(W\frac{K_{VS}}{K_{VSR}}\right) + s\left(\frac{K_{AS}+K_{VS}}{M}\right) + W\frac{K_{VS}}{M}\left(1+\frac{K_{AS}}{K_{VSR}}\right)} \tag{20}$$

The steady state term corresponding to the new configuration (Eq. 8) must be added to the transient term derived above. Thus, the complete suspension response after a switch in configuration is:

$$\left.\frac{X(s)}{Y(s)}\right| = \left.\frac{X(s)}{Y(s)}\right|_t + \left.\frac{X(s)}{Y(s)}\right|_s \tag{21}$$

Some simulations and tests have been carried out in order to assess the transient behaviour. Consider first the case in which a suspension with $C_r \approx 10^{-8}$ m^5/Ns is excited at its resonant frequency and, when $t = 2$s, the configuration is switched to that in which $C_r \approx 10^{-5}$ m^5/Ns. The analytical and experimental results are plotted in Fig. 10(a). It can be seen that the transient behaviour does not spread beyond two or three cycles and that the transient does not hinder the suspension performance. The same conclusions are reached when a suspension with $C_r \approx 10^{-5}$ m^5/Ns, excited

at its resonant frequency (Fig. 10(b)), is transformed, at $t = 2$s, into a new configuration in which $C_r \approx 10^{-8}$ m^5/Ns.

Other configurations and frequencies have been simulated and tested and the results, in terms of the time required to reach steady state conditions, have been summarized in Table 2. It can be seen that the delays are lower when switching from configurations of larger C_r's to configuration with smaller coefficients since the damping ratio is increased in the process. Table 2 also includes delays corresponding to transients that take place when both the chirp and the chain of harmonic signals are used as input.

7. Conclusions

A self adaptive pneumatic suspension has been presented, modeled and tested. The suspension employs a control strategy previously used for unbalanced machinery by the authors. As a step towards using the proposed strategy in more general situations, this paper considered two cases in which the type of input is known (piecewise harmonic or chirp) but the frequency needs to be estimated or identified. Algebraic predictors borrowed from other fields have proven to be extremely fast and accurate for this application. The strategy described in the paper relies on comparing the estimated

input frequency with the adaptive system transition frequency ω_{tr} which depends on the unknown value of sprung mass. Since in most practical cases the mass does not vary during vibration, a simple measuring technique has been devised in static conditions. Simulations and experiments show that the proposed control strategy greatly improves vibration isolation, and that the transient response when switching from one configuration to the other is very fast and does not hinder performance. The agreement between simulations and tests is quite remarkable.

8. Acknowledgement

The authors are grateful for the support received from the Regional Project PCI08-0082 titled "Análisis y diseño de elementos activos para el control de vibraciones" financed by the Consejería de Educación y Ciencia (Junta de Comunidades de Castilla-La Mancha). J.R. Trapero was supported by a Marie Curie Intra European Fellowship within the 7th European Union Framework Programme.

References

[1] Hostens I., Deprez K., Ramon H., "An improved design of air suspension for seats of mobile agricultural machines", Journal of Sound and Vibration 276 (2004), 141-156.

[2] Maciejewski I., Meyer L., Krzyzynski T. "Modelling and multi-criteria optimisation of passive seat suspension vibro-isolating properties", Journal of Sound and Vibration 324 (2009), pp. 520-538.

[3] Maciejewski I., Meyer L., Krzyzynski T. "The vibration damping effectiveness of an active seat suspension system and its robustness to varying mass loading", Journal of Sound and Vibration 329 (2010), pp. 3898-3914.

[4] Lee C.M., Bogatchenkov A.H., Goverdovskiy V.N., Shynkarenko Y.V., Temnikov A.I. "Position control of seat suspension with minimum stiffness", Journal of Sound and Vibration 292 (2006), pp. 435-442

[5] Ahn K.G., Pahk H.J., Jung M.Y., Cho D.W. "A hybrid-type active vibration isolation system using neural networks". Journal of Sound and Vibration, 192(4), (1996), 793-805.

[6] Kim Y.B., Yi H.B., Lee B.K."Design and application of magnetic damper for reducing rotor vibration". International Korean Society of Mechanical Engineers Journal, 24, (2000), 355-361.

[7] Kim Y.B., Hwang W.G., Kee C.D., Yi H.B."Active vibration control of a suspension system using an electromagnetic damper". Proceedings of the Institution of Mechanical Engineers, Part D. (2001), 865-873.

[8] K. Nakano, Y. Suda, S. Nakadai, "Self-powered active vibration control using a single electric actuator", Journal of Sound and Vibration, 260, (2003), 213-235.

[9] J. Alony, S. Sankar "A new concept in semi-active vibration isolation", American Society of Mechanical Engineers, 109, (1987), 242-247.

[10] X. Wu, M.J. Griffin, "A semi-active control policy to reduce the occurrence and severity of end-stop impacts in a suspension seat with an electrorheological fluid", Journal of Sound and Vibration, 203, (1997), 781-793.

[11] J-D. Wu. R.J. Chen, "Application of an active controller for reducing small-amplitude verticalvibration in a vehicle seat", Journal of Sound and Vibration, 274, (2004), 939-951.

[12] Y. Ohtani, T. Yoshimura, "Fuzzy control of a manipulator using the concept of sliding mode", International Journal of Systems Science, 27, (1996), 179-186.

[13] T. Yoshimura, A. Kume, M. Kurimoto, J. Hino, "Construction of an active suspension system of a quarter car model using the concept of sliding mode control", Journal of Sound and Vibration, 239(2), (2001), 187-199.

[14] M. Fliess, H. Sira-Ramirez, "An algebraic framework for linear identification", European Series in Applied and Industrial Mathematics: Control Optimisation and Calculus of Variations, 9, (2003), 151-168.

[15] M. Fliess, H. Sira-Ramírez, "Closed-loop parametric identification for continuous-time linear systems via new algebraic techniques", Identification of continuous-time models from sampled data, 363-391, London, Springer, (2008).

[16] J. R. Trapero-Arenas, H. Sira-Ramírez, V. Feliu-Batlle. "A fast on-line frequency estimator of lightly damped vibrations in flexible structures", Journal of Sound and Vibration, 307, (2007), 365-378.

[17] J. Becedas, J.R. Trapero, V. Feliu, H. Sira-Ramírez, "Adaptive con-

troller for single-link flexible manipulators based on algebraic identification and generalized proportional integral control", IEEE Transactions on Systems, Man and Cybernetics-Part B, 39, (2009), 735-751.

[18] E. Pereira, J.R. Trapero, I. M. Díaz, V. Feliu, "Adaptive input shaping for manoeuvring flexible structures using an algebraic identification technique", Automatica, 45, (2009), 1046-1051.

[19] J. R. Trapero, H. Sira-Ramírez, V. Feliu-Batlle, "An algebraic frequency estimator for a biased and noisy sinusoidal signal", Signal Processing, 87, (2007), 1188-1201.

[20] M. Fliess, M. Mboup, H. Mounier, H. Sira-Ramírez, "Questioning some paradigms of signal processing via concrete examples", Mexico City, Editorial Lagares, (2003).

[21] A.J. Nieto, A.L. Morales, A. González, J.M. Chicharro, P. Pintado, "An analytical model of pneumatic suspensions based on an experimental characterization", Journal of Sound and Vibration, 313 (1-2), (2008), 290-307.

[22] C. Erin, B.Wilson, J. Zapfe, "An improved model of a pneumatic vibra-

tion isolator: theory and experiment", Journal of Sound and Vibration, 218 (1), (1998), 81-101.

[23] I.H.Shames, "Mechanics of fluids", Second edition. McGraw-Hill, (1982).

[24] A.J. Nieto, A.L. Morales, J.M. Chicharro, P. Pintado, "Unbalanced machinery vibration isolation with a semi-active pneumatic suspension", Journal of Sound and Vibration, 329 (1), (2010), 3-12.

[25] M. Mboup, "Parameter estimation via differential algebra and operational calculus", (online http://hal.inria.fr/inria-00138294/en/).

[26] J. Trapero-Arenas, M. Mboup, E. Pereira-Gonzalez, V. Feliu,"On-line frequency and damping estimation in a single-link flexible manipulator based on algebraic identification" in Proc. 16th Mediterranean Conf. Control Autom., Jun. 2008, pp. 338-343.

[27] K. Kanazawa, K. Hirata, "Parametric estimation of the cross-power spectral density", Journal of Sound and Vibration, 282, (2005), 1-35.

Figure captions

Figure 1. Pneumatic suspension: (a) scheme, (b) experimental workbench.

Figure 2. Suspension transmissibility (simulation).

Figure 3. Effect of suspension parameters on: (a) stiffness, (b) transmissibility. Thick solid lines: $V_r = 24\ l$, $V_s^{st} = 0.55\ l$, $A_s^{st} = 4.5 \cdot 10^{-3}\ m^2$, $\lambda = -9 \cdot 10^{-2}\ m$, $\kappa = 9 \cdot 10^{-3}\ m^2$. Thin solid lines: $V_r = 2\ l$, $V_s^{st} = 1.4\ l$, $A_s^{st} = 1.05 \cdot 10^{-2}\ m^2$, $\lambda = 0.1\ m$, $\kappa = 0.01\ m^2$.

Figure 4. (a) Influence of sprung mass on ω_{tr}, (b) regression curves for the determination of the sprung mass.

Figure 5. (a) Noisy harmonic signal, (b) Estimated frequency (solid line) and correct frequency (dashed line).

Figure 6. (a) Noisy Chirp signal, (b) Estimated ϕ_1 and its correct value, (c) Estimated ϕ_2 and its correct value, (d) Instantaneous frequency ($\varphi_1 + 2\varphi_2 t$).

Figure 7. Control scheme for the pneumatic suspension.

Figure 8. (a) Piecewise harmonic signal with uniform normal noise, (b) frequency estimation, (c) numerical comparison between passive and adaptive modes, (d) experimental comparisons.

Figure 9. (a) Chirp signal (0.5-10 Hz), (b) instantaneous frequency estimation, (c) passive response, (d) Numerical adaptive response, (e) experimental

adaptive response.

Figure 10. Study of transients (a) switching from $C_r \approx 10^{-8}$ to $C_r \approx 10^{-5}$, (b) switching from $C_r \approx 10^{-5}$ to $C_r \approx 10^{-8}$.

Tables

Table 1. Summary of pneumatic suspension data.

Table 2. Time delay when switching between configurations.

Table 1: Summary of pneumatic suspension data.

Parameter	Value
V_r	24 l
V_s^{st}	0.55 l
A_s^{st}	4.5 10^{-3} m^2
λ	-9 10^{-2} m
κ	9 10^{-3} m^2

Table 2: Time delay when switching between configurations.

Transient	Method	Delay
Switch: $C_r \approx 10^{-8} \Rightarrow C_r \approx 10^{-5}$ Harmonic input, frequency: f_n of $C_r \approx 10^{-8}$ Response: Fig. 10(a)	Experimental Model	0.98 s 0.87 s
Switch: $C_r \approx 10^{-5} \Rightarrow C_r \approx 10^{-8}$ Harmonic input, frequency: f_n of $C_r \approx 10^{-5}$ Response: Fig. 10(b)	Experimental Model	0.89 s 0.82 s
Switch: $C_r \approx 10^{-8} \Rightarrow C_r \approx 10^{-5}$ Input: chirp signal Fig. 9(a) Response: Figs. 9(d) and 9(e)	Experimental Model	1.14 s 1.07 s
Switch: $C_r \approx 10^{-8} \Rightarrow C_r \approx 10^{-5}$ Input: piecewise harmonic signal Fig. 8(a) Response: Figs. 8(c) and 8(d)	Experimental Model	0.67 s 0.75 s
Switch: $C_r \approx 10^{-5} \Rightarrow C_r \approx 10^{-8}$ Input: piecewise harmonic signal Fig. 8(a) Response: Figs. 8(c) and 8(d)	Experimental Model	0.48 s 0.43 s

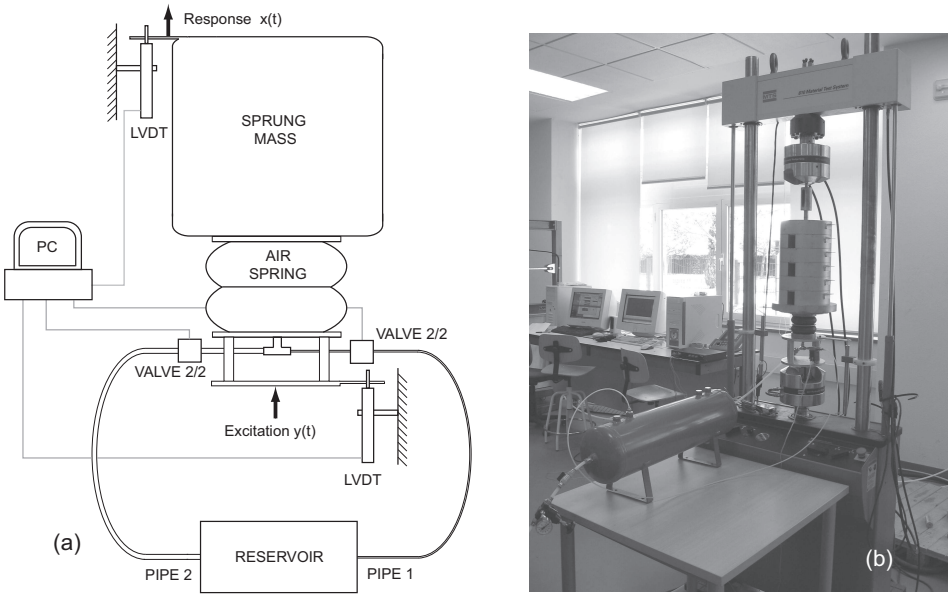

Figure 1: Pneumatic suspension: (a) scheme, (b) experimental workbench.

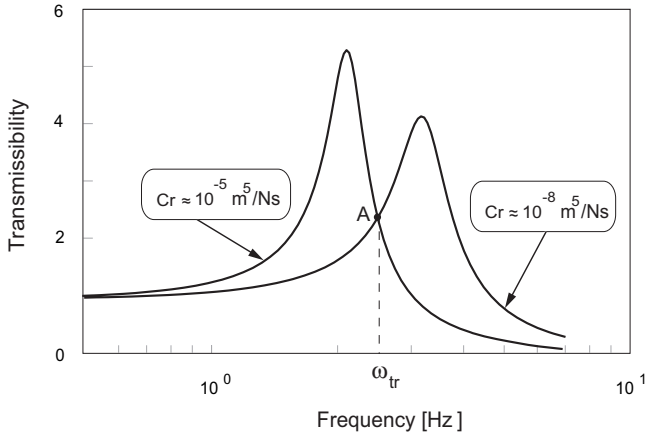

Figure 2: Suspension transmissibility (simulation).

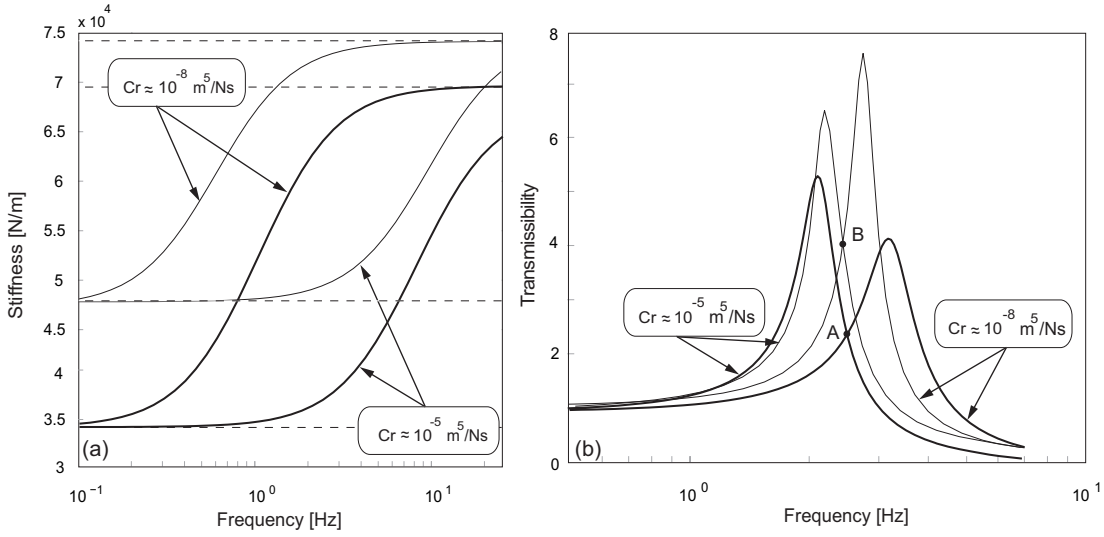

Figure 3: Effect of suspension parameters on: (a) stiffness, (b) transmissibility. Thick solid lines: $V_r = 24\ l$, $V_s^{st} = 0.55\ l$, $A_s^{st} = 4.5 \cdot 10^{-3}\ m^2$, $\lambda = -9 \cdot 10^{-2}\ m$, $\kappa = 9 \cdot 10^{-3}\ m^2$. Thin solid lines: $V_r = 2\ l$, $V_s^{st} = 1.4\ l$, $A_s^{st} = 1.05 \cdot 10^{-2}\ m^2$, $\lambda = 0.1\ m$, $\kappa = 0.01\ m^2$.

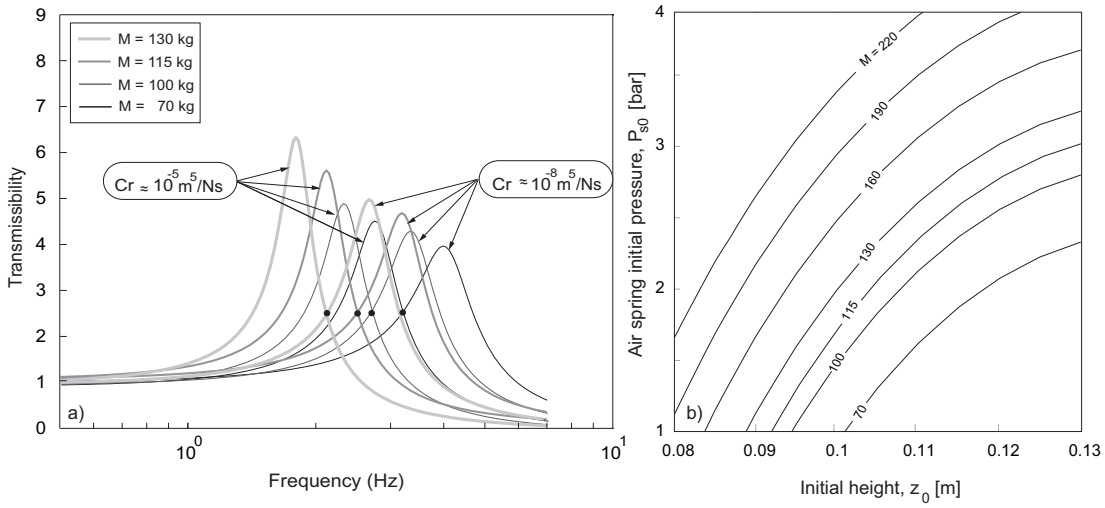

Figure 4: (a) Influence of sprung mass on ω_{tr}, (b) regression curves for the determination of the sprung mass.

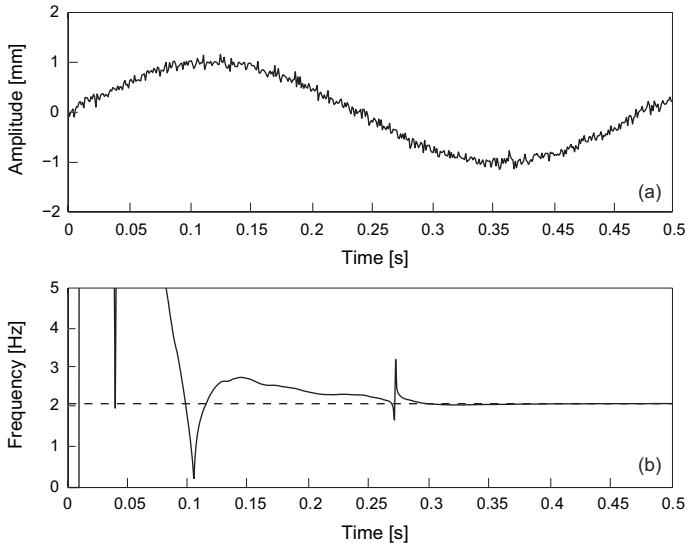

Figure 5: (a) Noisy harmonic signal, (b) Estimated frequency (solid line) and correct frequency (dashed line).

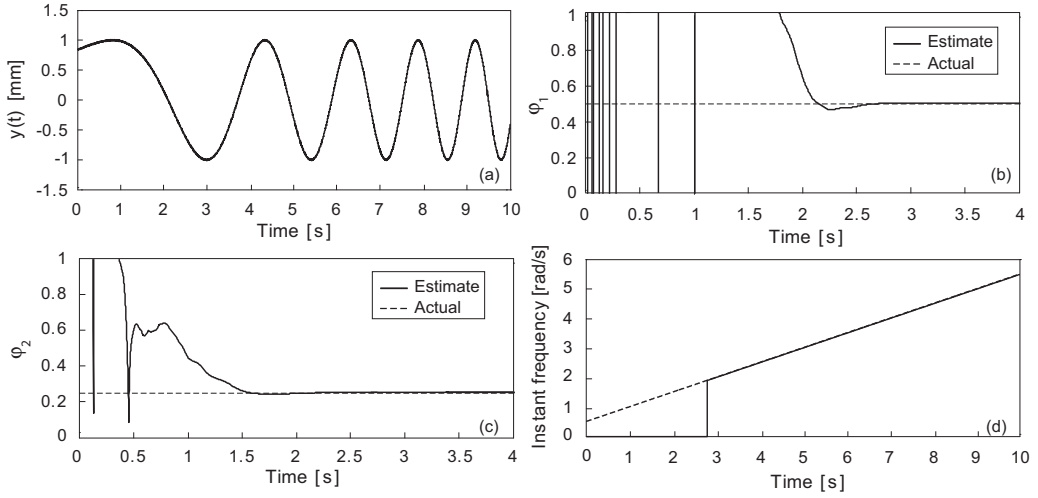

Figure 6: (a) Noisy Chirp signal, (b) Estimated ϕ_1 and its correct value, (c) Estimated ϕ_2 and its correct value, (d) Instantaneous frequency $(\varphi_1 + 2\varphi_2 t)$.

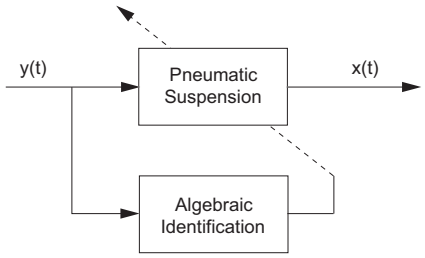

Figure 7: Control scheme for the pneumatic suspension.

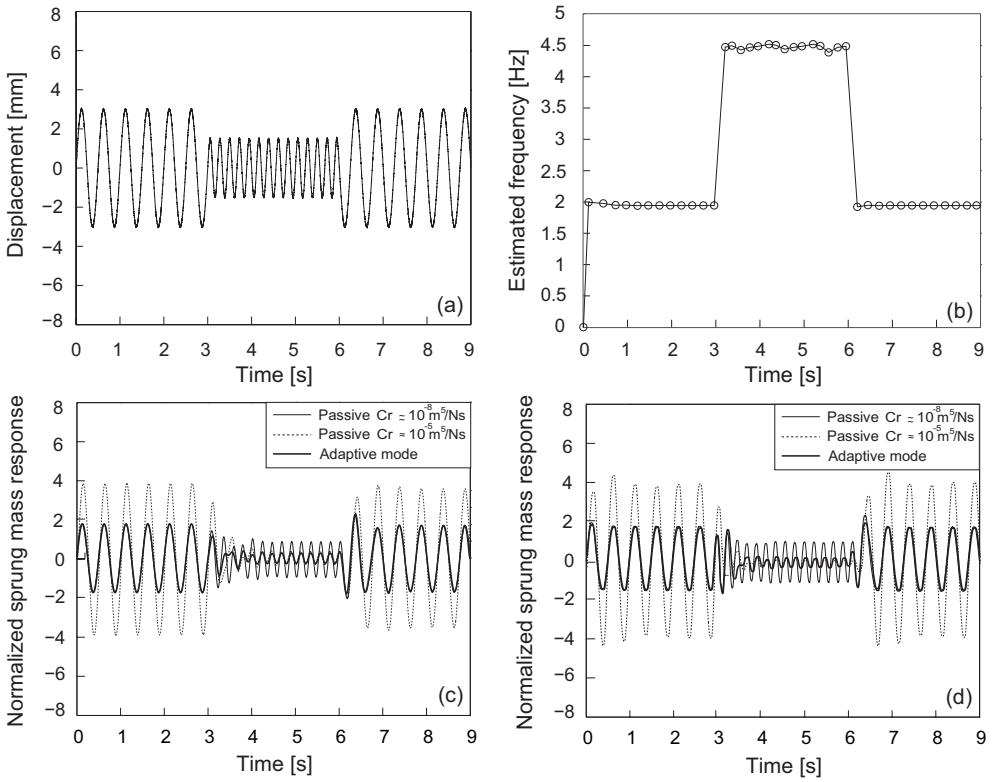

Figure 8: (a) Piecewise harmonic signal with uniform normal noise, (b) frequency estimation, (c) numerical comparison between passive and adaptive modes, (d) experimental comparisons.

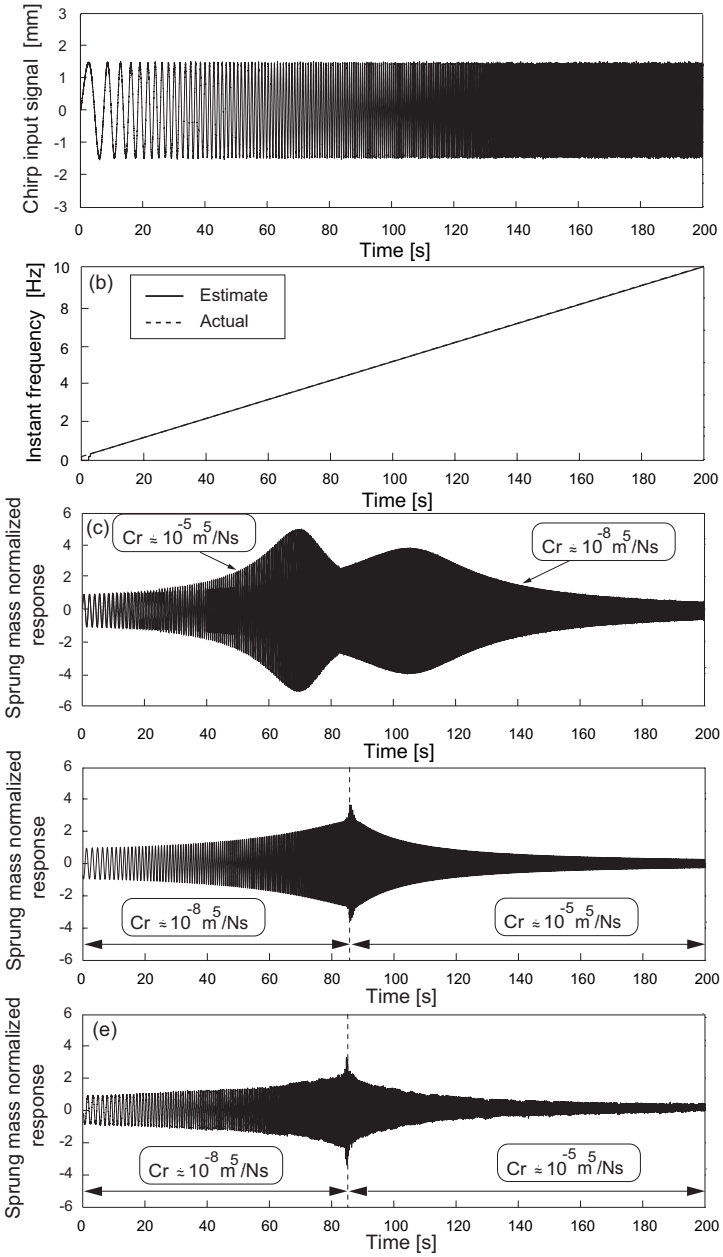

Figure 9: (a) Chirp signal (0.5-10 Hz), (b) instantaneous frequency estimation, (c) passive response, (d) Numerical adaptive response, (e) experimental adaptive response.

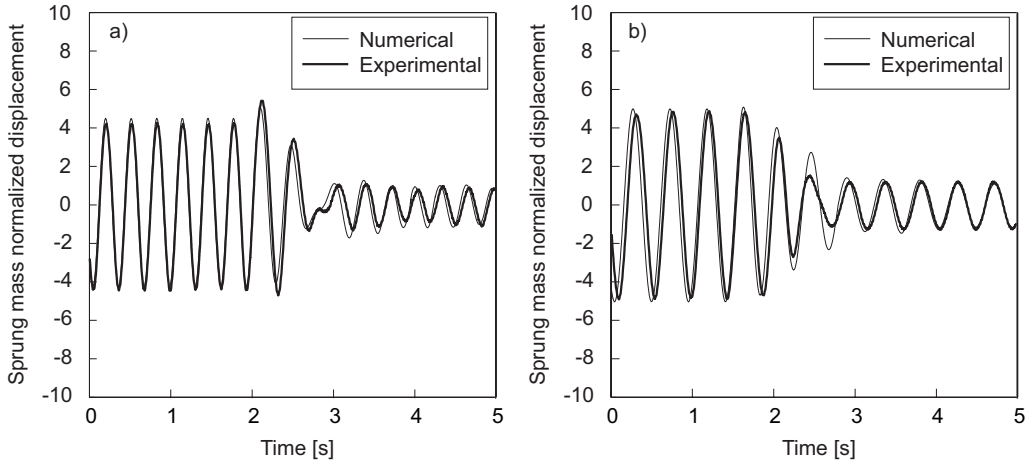

Figure 10: Study of transients (a) switching from $C_r \approx 10^{-8}$ to $C_r \approx 10^{-5}$, (b) switching from $C_r \approx 10^{-5}$ to $C_r \approx 10^{-8}$.